

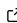


1 atems: Analysis tools for TEM images of
2 carbonaceous particles

3 Timothy A Sipkens ^{1,2}✉, Ramin Dastanpour¹, Una Trivanovic ¹, Hamed
4 Nikookar¹, and Steven N. Rogak ¹

5 ¹ Mechanical Engineering, University of British Columbia, Canada ² Metrology Research Centre,
6 National Research Council Canada, Canada ✉ Corresponding author

DOI: [10.xxxxxx/draft](https://doi.org/10.xxxxxx/draft)

Software

- [Review](#) 
- [Repository](#) 
- [Archive](#) 

Editor: [Renata Diaz](#) 

Reviewers:

- [@jonbmartin](#)
- [@tytell](#)

Submitted: 10 October 2023

Published: unpublished

License

Authors of papers retain copyright and release the work under a Creative Commons Attribution 4.0 International License ([CC BY 4.0](#)).

7 **Summary**

8 The objective of atems is to provide a suite of open source analysis tools (largely in Matlab)
9 for transmission electron microscopy (TEM) image analysis that are specifically designed for
10 soot and related carbonaceous particles (e.g., tarballs). This codebase started as a manual
11 analysis code by Dastanpour & Rogak (2014), with the first automated methods added by
12 Dastanpour et al. (2016). The current, open source version has been streamlined and expanded
13 to include a larger suite of automated analysis methods from the literature, as detailed in the
14 following section. In this regard, a key contribution of this codebase is to provide open source
15 implementations of multiple analysis methods spanning a range of laboratories. This codebase
16 places these methods in the same framework, with the goal of enabling intercomparisons of
17 analysis routines across a range of data.

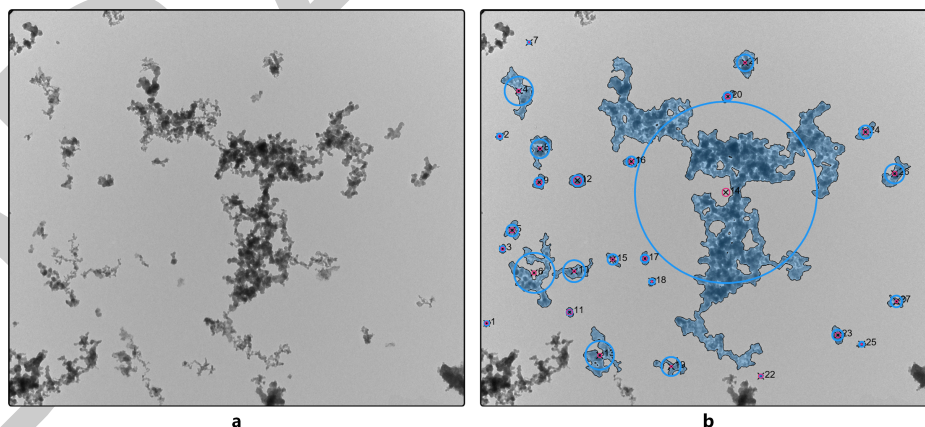


Figure 1: Sample TEM image of soot demonstrating the aggregate structure, where a is an unlabeled image containing soot aggregates and b is that same image with the aggregates labeled.

18 **Statement of need**

19 Soot, carbon black, and other carbonaceous particles have important climate, health, and
20 technological impacts that depend on their morphology. These particles have complex shapes
21 composed of a collection of small, primary particles in fractal arrangements, as shown in
22 [Figure 1a](#). TEM images of these particles allow for detailed information about particle
23 morphology that is unavailable in other characterization techniques. However, extracting
24 this information requires image analysis across a statistically-significant number of particles,

25 with the quality of conclusions improving as the number of characterized particles increases.
 26 For instance, Kelesidis et al. (2020) suggested quantifying at least 400 primary particles per
 27 experimental condition in a premixed flame to get an accurate average primary particle diameter
 28 from manually drawing ellipses (that study counted 800 primary particles). In the broader
 29 literature, a few hundred particles per condition seems to be standard, with other authors
 30 having employed between 150 and 400 particles per condition (Liati et al., 2014; Marhaba
 31 et al., 2019; Trivanovic et al., 2019, 2020), depending on the type of analysis. For multiple
 32 conditions, this can quickly expand to over 1000 particles. This characterization is often done
 33 manually, which at a minimum of several minutes per aggregate, is incredibly labour intensive.
 34 Unfortunately, the low contrast (carbonaceous particles on carbon films) and complex particle
 35 morphology of common carbonaceous particles makes automated analysis challenging, requiring
 36 unique analysis methods over those developed for traditional TEM image analysis of many
 37 engineered nanomaterials (Schneider et al., 2012). At the same time, existing automated
 38 methods across the literature are typically only applied to data from a single laboratory, with
 39 few exceptions (Anderson et al., 2017; Sipkens et al., 2021). This limits comparability between
 40 laboratories (Sipkens et al., 2023).

41 Methods

42 After loading images (with an automated method provided for doing so), analysis involves two
 43 major steps.

44 The first step is segmentation of the aggregates from their background. Available methods
 45 include the slider-based manual approach of Dastanpour & Rogak (2014); the common Otsu
 46 method; a modification of Otsu by Dastanpour et al. (2016) that employs morphological
 47 operations to improve segmentation; the *k*-means approach of Sipkens & Rogak (2021); and
 48 carboseg, which is the convolutional neural network (CNN) approach from Sipkens et al.
 49 (2021). Functionality is also available to prepare (e.g., read and crop image footers) and
 50 export images for external analysis, prior to reading the images in for subsequent analysis.
 51 This enables external extensions, such as the WEKA segmentation method of Altenhoff et al.
 52 (2020). Tools are then available to compute aggregate projected area, perimeter, and
 53 circularity, among other properties. A sampling of segmentations produced by these methods
 54 is presented in Figure 2.

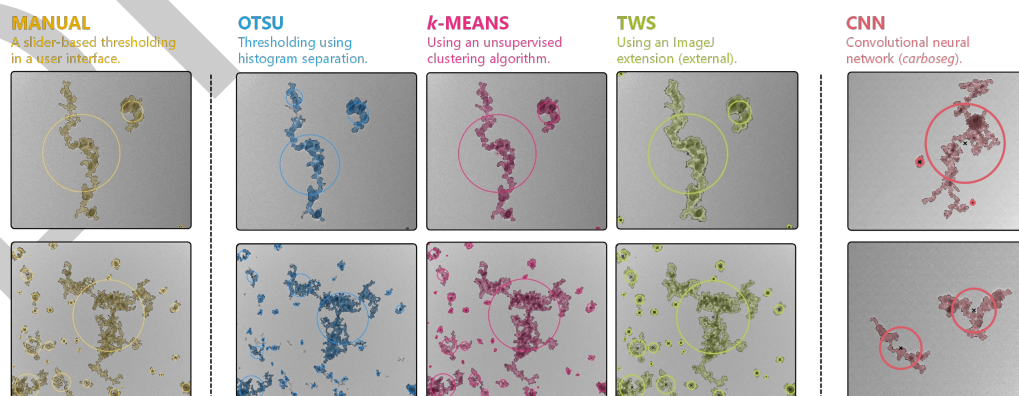


Figure 2: Sample segmentations across a range of methods available in this code. The manual method corresponds to an updated version of the code development by Dastanpour et al. (2016). The Otsu segmentation is standard Otsu, without any adaptations. The *k*-means method is that described by Sipkens & Rogak (2021). TWS refers to trainable WEKA segmentation based on the method described by Altenhoff et al. (2020), which makes use of the code enabling external extensions. These first four panels correspond to images from Sipkens & Rogak (2021). The final panel corresponds to the convolutional neural network method described by Sipkens et al. (2021).

55 Second, this code works to identify primary particles, that is the small, roughly circular
56 structures inside the aggregates. Available methods include a updated version of the Euclidean
57 distance mapping–surface-based scale analysis (EDM-SBS) of Bescond et al. (2014), converted
58 from SciLab to Matlab in association with Sipkens et al. (2021) (functionality between the two
59 languages resulted in minor differences); the Euclidean distance mapping–watershed (EDM-WS)
60 method of De Temmerman et al. (2014); the pair correlation method (PCM) of Dastanpour
61 et al. (2016); the Hough transform method of Kook et al. (2016); and the Hough transform
62 method of Altenhoff et al. (2020).

63 General plotting and other utilities (`tools.*`) are provided to enable further analysis and
64 visualization (e.g., as in Figure 1b and Figure 2).

65 Use

66 This code has been used in a number of studies in the literature. This code was used by
67 Sipkens et al. (2021) to compare multiple segmentation and primary particle analysis methods.
68 The code was also used by Trivanovic et al. (2019), Kheirkhah et al. (2020), and Trivanovic
69 et al. (2020) to perform image analysis of marine engine and flare soot. The *k*-means method
70 in this code (Sipkens & Rogak, 2021) was also employed for soot by Li (2022).

71 Acknowledgements

72 We wish to acknowledge related code released in association with some of the cited work.
73 These including Matlab code provided in Kook et al. (2016) and SciLab code released in
74 association with Bescond et al. (2014). The code from Altenhoff et al. (2020) was provided
75 by the authors and adapted to the present format.

76 We also wish to acknowledge funding by the Canadian Council of the Arts (Killam Fellowship),
77 the Natural Sciences and Engineering Research Council of Canada (NSERC), and Transport
78 Canada.

79 References

- 80 Altenhoff, M., Abmann, S., Teige, C., Huber, F. J. T., & Will, S. (2020). An opti-
81 mized evaluation strategy for a comprehensive morphological soot nanoparticle aggre-
82 gate characterization by electron microscopy. *Journal of Aerosol Science*, *139*, 105470.
83 <https://doi.org/10.1016/j.jaerosci.2019.105470>
- 84 Anderson, P. M., Guo, H., & Sunderland, P. B. (2017). Repeatability and reproducibility
85 of TEM soot primary particle size measurements and comparison of automated methods.
86 *Journal of Aerosol Science*, *114*, 317–326. <https://doi.org/10.1016/j.jaerosci.2017.10.002>
- 87 Bescond, A., Yon, J., Ouf, F. X., Ferry, D., Delhayé, D., Gaffié, D., Coppalle, A., & Rozé, C.
88 (2014). Automated determination of aggregate primary particle size distribution by TEM
89 Image Analysis: Application to soot. *Aerosol Science and Technology*, *48*(8), 831–841.
90 <https://doi.org/10.1080/02786826.2014.932896>
- 91 Dastanpour, R., Boone, J. M., & Rogak, S. N. (2016). Automated primary particle sizing
92 of nanoparticle aggregates by TEM image analysis. *Powder Technology*, *295*, 218–224.
93 <https://doi.org/10.1016/j.powtec.2016.03.027>
- 94 Dastanpour, R., & Rogak, S. N. (2014). Observations of a correlation between primary particle
95 and aggregate size for soot particles. *Aerosol Science and Technology*, *48*(10), 1043–1049.
96 <https://doi.org/10.1080/02786826.2014.955565>

- 97 De Temmerman, P.-J., Verleysen, E., Lammertyn, J., & Mast, J. (2014). Semi-automatic size
98 measurement of primary particles in aggregated nanomaterials by transmission electron
99 microscopy. *Powder Technology*, 261, 191–200. [https://doi.org/10.1016/j.powtec.2014.04.](https://doi.org/10.1016/j.powtec.2014.04.040)
100 [040](https://doi.org/10.1016/j.powtec.2014.04.040)
- 101 Kelesidis, G. A., Kholghy, M. R., Zuercher, J., Robertz, J., Allemann, M., Duric, A., & Pratsinis,
102 S. E. (2020). Light scattering from nanoparticle agglomerates. *Powder Technology*, 365,
103 52–59. <https://doi.org/10.1016/j.powtec.2019.02.003>
- 104 Kheirkhah, P., Baldelli, A., Kirchen, P., & Rogak, S. (2020). Development and validation of
105 a multi-angle light scattering method for fast engine soot mass and size measurements.
106 *Aerosol Science and Technology*, 54(9), 1083–1101. [https://doi.org/10.1080/02786826.](https://doi.org/10.1080/02786826.2020.1758623)
107 [2020.1758623](https://doi.org/10.1080/02786826.2020.1758623)
- 108 Kook, S., Zhang, R., Chan, Q. N., Aizawa, T., Kondo, K., Pickett, L. M., Cenker, E.,
109 Bruneaux, G., Andersson, O., Pagels, J., & Z., N. E. (2016). Automated detection of
110 primary particles from transmission electron microscope (TEM) images of soot aggregates
111 in diesel engine environments. *SAE International Journal of Engines*, 9(1), 279–296.
112 <https://doi.org/10.4271/2015-01-1991>
- 113 Li, Y. (2022). *Flame and smoke characterization in reduced gravity for enhanced spacecraft*
114 *safety* [PhD thesis]. Sorbonne Université.
- 115 Liati, A., Brem, B. T., Durdina, L., Vögtli, M., Arroyo Rojas Dasilva, Y., Dimopoulos
116 Eggenschwiler, P., & Wang, J. (2014). Electron microscopic study of soot particulate
117 matter emissions from aircraft turbine engines. *Environmental Science & Technology*,
118 48(18), 10975–10983. <https://doi.org/10.1021/es501809b>
- 119 Marhaba, I., Ferry, D., Laffon, C., Regier, T. Z., Ouf, F.-X., & Parent, P. (2019). Aircraft
120 and MiniCAST soot at the nanoscale. *Combustion and Flame*, 204, 278–289. <https://doi.org/10.1016/j.combustflame.2019.03.018>
- 122 Schneider, C. A., Rasband, W. S., & Eliceiri, K. W. (2012). NIH image to ImageJ: 25 years of
123 image analysis. *Nature Methods*, 9(7), 671–675. <https://doi.org/10.1038/nmeth.2089>
- 124 Sipkens, T. A., Boies, A., Corbin, J. C., Chakrabarty, R. K., Olfert, J. S., & Rogak, S. N.
125 (2023). Overview of methods to characterize the mass, size, and morphology of soot.
126 *Journal of Aerosol Science*, 173, 106211. <https://doi.org/10.1016/j.jaerosci.2023.106211>
- 127 Sipkens, T. A., Frei, M., Baldelli, A., Kirchen, P., Kruis, F. E., & Rogak, S. N. (2021). Char-
128 acterizing soot in TEM images using a convolutional neural network. *Powder Technology*,
129 387, 313–324. <https://doi.org/10.1016/j.powtec.2021.04.026>
- 130 Sipkens, T. A., & Rogak, S. N. (2021). Using k-means to identify soot aggregates in
131 transmission electron microscopy images. *Journal of Aerosol Science*, 152, 105699. <https://doi.org/10.1016/j.jaerosci.2020.105699>
- 133 Trivanovic, U., Corbin, J. C., Baldelli, A., Peng, W., Yang, J., Kirchen, P., Miller, J. W.,
134 Lobo, P., Gagné, S., & Rogak, S. N. (2019). Size and morphology of soot produced by
135 a dual-fuel marine engine. *Journal of Aerosol Science*, 138, 105448. [https://doi.org/10.](https://doi.org/10.1016/j.jaerosci.2019.105448)
136 [1016/j.jaerosci.2019.105448](https://doi.org/10.1016/j.jaerosci.2019.105448)
- 137 Trivanovic, U., Sipkens, T. A., Kazemimanesh, M., Baldelli, A., Jefferson, A. M., Conrad, B.
138 M., Johnson, M. R., Corbin, J. C., Olfert, J. S., & Rogak, S. N. (2020). Morphology and
139 size of soot from gas flares as a function of fuel and water addition. *Fuel*, 279, 118478.
140 <https://doi.org/10.1016/j.fuel.2020.118478>